

Albert A. Ruth, Uwe Heitmann, Elke Heinecke, and  
Christa Fittschen\*

# The Rotationally-Resolved Absorption Spectrum of Formaldehyde from 6547 to 7051 cm<sup>-1</sup>

DOI 10.1515/zpch-2015-0623

Received April 7, 2015; accepted July 28, 2015

**Abstract:** We report new experimental data on the rotationally resolved room temperature absorption spectrum of CH<sub>2</sub>O in the near infrared (NIR) region between 6804 and 7051 cm<sup>-1</sup> (1470–1418 nm). Data have been obtained by cavity enhanced absorption spectroscopy and complement the spectrum in the wavelength range 6547–6804 cm<sup>-1</sup>, obtained using virtually the same experimental set-up and already published in an earlier publication (Staak et al., *J. Mol. Spectrosc.* **229** (2005) 115–121). Several vibrational combination bands occur in this region and give rise to a congested spectrum and over 4500 lines with cross-sections over  $5 \times 10^{-23}$  cm<sup>2</sup> were observed. Recent experimental studies using NIR absorption spectroscopy for quantifying CH<sub>2</sub>O in different chemical systems indicate that the absorption cross-sections obtained by Staak et al. may have been overestimated. The results of these experiments are reviewed here and a recommendation for absolute absorption cross sections of CH<sub>2</sub>O in the NIR range will be given. Absolute absorption cross-sections stated here are corrected by the recommended factor.

**Keywords:** Spectroscopy, Formaldehyde, Near Infrared, Cavity Enhanced Spectroscopy.

---

\*Corresponding author: Christa Fittschen, Université de Lille, PhysicoChimie des Processus de Combustion et de l'Atmosphère (PC2A) UMR 8522, CNRS/Lille 1, Cité scientifique, 59655 Villeneuve d'Ascq Cedex, France, e-mail: christa.fittschen@univ-lille1.fr

**Albert A. Ruth:** Physics Department & Environmental Research Institute, University College Cork, Cork, Ireland

**Uwe Heitmann:** Physics Department & Environmental Research Institute, University College Cork, Cork, Ireland; and Technische Universität Berlin, Institut für Optik und Atomare Physik, Sekr. EW3-1, Hardenbergstr. 36, 10623 Berlin, Germany

**Elke Heinecke:** Freie Universität Berlin, Fachbereich Physik, Arnimallee 14, 14195 Berlin, Germany

---

Dedicated to Prof. Dr. Dr. h.c. mult. Jürgen Troe on the occasion of his 75<sup>th</sup> birthday

## 1 Introduction

Formaldehyde ( $\text{CH}_2\text{O}$ ) is an important intermediate in the oxidation of most hydrocarbons and plays a key role in chemistry of the atmosphere due to efficient photolysis of  $\text{CH}_2\text{O}$  at wavelengths below 360 nm [1, 2]. For example, the reaction of  $\text{O}_2$  with the products (H and HCO) of formaldehyde photolysis below  $\sim 329$  nm leads to the formation of  $\text{HO}_2$  radicals [3]. Thus photolysis of  $\text{CH}_2\text{O}$  maintains the oxidizing capacity of the atmosphere. Large efforts have been made in order to develop reliable detection methods of  $\text{CH}_2\text{O}$ . For the quantification of  $\text{CH}_2\text{O}$  under *atmospheric conditions* with ground-based or airborne instruments absorption spectroscopy has been extensively used, predominantly in two distinct wavelength regions: (i) the UV region between 260–350 nm [4–8], and (ii) the infrared (IR) region [9–12], either around  $3.5\text{ }\mu\text{m}$ , or between  $5\text{--}6\text{ }\mu\text{m}$ . Absorption cross-sections in the IR regions are rather large and thus enable high detection sensitivity. A comprehensive overview and intercomparison of absorption cross-section data in these wavelength ranges has been given by Gratien et al. [13]. Under *laboratory conditions*,  $\text{CH}_2\text{O}$  has also been quantified either by UV-absorption or using tunable diode laser absorption spectroscopy (TDLAS) in the infrared region [14–17]. The near infrared (NIR) region, however, where much weaker overtone or combination bands can be found, has only moved into the focus of interest due to the significant sensitivity improvements that were made with cavity-enhanced spectroscopic techniques over the last two decades. Even though the NIR is not a wavelength region specifically useful for the quantification of  $\text{CH}_2\text{O}$  in the atmosphere, it is nevertheless a wavelength region that finds more and more applications in laboratory studies thanks to the development of reliable cavity methods and the corresponding, widely available optical components.

As for absorption features of  $\text{CH}_2\text{O}$  in the NIR range, Barry et al. [18–20] measured absolute absorption cross-sections of selected lines in the  $2\nu_5$  transition around  $5680\text{ cm}^{-1}$  using two methods; cavity ring-down spectroscopy (CRDS), and cavity-enhanced absorption spectroscopy (CEAS). They reported good agreement between the absorption cross-sections obtained by the two different approaches. Zhao et al. [21] measured a spectrum at somewhat higher energies, i.e. from  $6351\text{--}6362\text{ cm}^{-1}$ , using cavity-enhanced absorption spectroscopy (CEAS). Previously, Staak et al. [22] measured the absorption spectrum of  $\text{CH}_2\text{O}$  in the range  $6547\text{--}6804\text{ cm}^{-1}$ , where transitions of several combination bands can be

found [23]. cw-CRDS has been used more recently in several absorption experiments of several individual lines in the region around 6600 cm<sup>-1</sup> [24–28] for the direct and indirect quantification of CH<sub>2</sub>O.

In the context of the available NIR absorption measurements the aim of this publication is twofold: Firstly, unpublished absorption data are presented that extend the absorption spectrum in Ref. [22] by ~250 cm<sup>-1</sup> towards higher energies: these data had been obtained at the same time using the same set-up as the data in Ref [22], but had not yet been published. Secondly, even though the direct and indirect evaluations of the CH<sub>2</sub>O absorption in Refs. [24–28] confirmed line positions in Ref. [22], discrepancies in the absolute cross-sections of up to a factor of 2 were reported. This publication reviews and scrutinized the relevant literature in order to establish new recommendations of absorption cross-sections for the spectral region from 6547–7051 cm<sup>-1</sup>. The absorption data and information on cross-sections of CH<sub>2</sub>O presented here are useful for the development of theoretical models of the ground state potential of CH<sub>2</sub>O and for future observation and quantification of CH<sub>2</sub>O in the NIR region.

## 2 Experimental

Cavity-enhanced absorption spectroscopy was used to measure the rotationally-resolved formaldehyde spectrum between 6547 and 6804 cm<sup>-1</sup> by Staak et al. [22], and between 6800 and 7051 cm<sup>-1</sup> in the present work. The main components of the experimental setup have been published before and can be found in Figure 1 of Refs. [22, 29, 30]. The experimental description given here refers to the new measurements in the region 6800–7051 cm<sup>-1</sup> (i.e. ~1470–1418 nm). This spectral range was covered with a temperature-stabilized external cavity diode laser (Sacher Lasertechnik, TEC500) in Littman configuration. The laser had a bandwidth of ~1 MHz and was operated at typical powers of ~4 mW. An optical isolator was used to reduce feedback into the laser and to prevent the associated laser instability. The distance from the well-collimated laser to the cavity was also made as large as possible (ca. 2.3 m) for the same reason. The cavity was formed by two dielectric spherical mirrors (radius of curvature  $r = -3$  m, maximum reflectivity  $R \sim 0.9975$ ) separated by 85 cm. As opposed to the measurements in Staak et al. [22] the present data were established using off-axis alignment (OA-CEAS) [31]; i.e. the laser beam entered the cavity parallel to the optical axis ~8 mm away from the center of the cavity's entrance mirror. The laser was repeatedly scanned mode-hop free over overlapping wavenumber intervals of ~2 cm<sup>-1</sup>; the intervals were subsequently concatenated to yield the

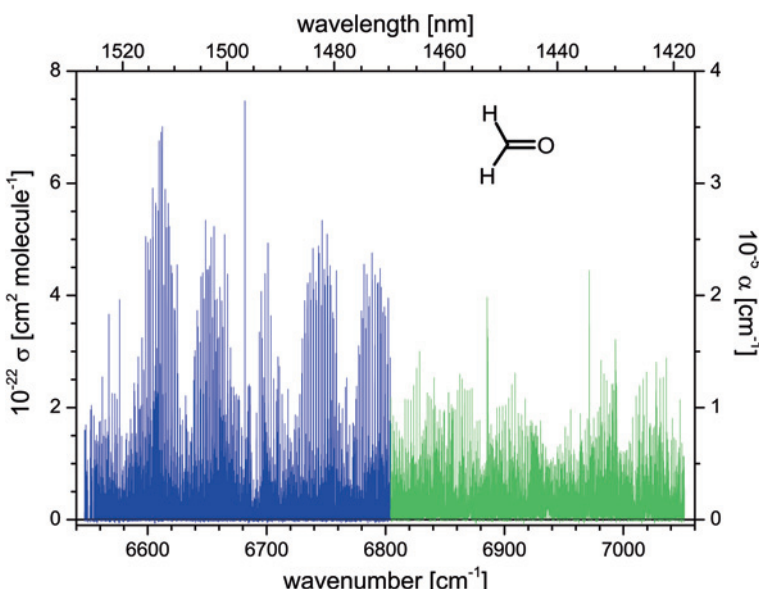


**Figure 1:** Room temperature near-infrared absorption spectrum of formaldehyde at 2 mbar between  $6547\text{ cm}^{-1}$  and  $7051\text{ cm}^{-1}$ . Data from  $6547\text{--}6804\text{ cm}^{-1}$  are taken from Staak et al. and divided by a factor of 2.

overall spectrum. The light transmitted through the cavity was detected with an InGaAs photodiode (NewFocus, Nirvana 2017). The data were collected and averaged with a digital oscilloscope (LeCroy Waverunner LT264) over 500 sweeps per interval. The typical overall acquisition time was 55 s at a sampling rate of 9 Hz. The minimum detectable absorption for these conditions was better than  $5 \times 10^{-7}\text{ cm}^{-1}$ . The sampling interval of  $\sim 0.0008\text{ cm}^{-1}$  was enough to resolve the  $\text{CH}_2\text{O}$  Doppler-broadened FWHM of about  $0.015\text{ cm}^{-1}$ . The wavenumber calibration was based on (i) simultaneous measurement of absorption line positions of 10 mbar  $\text{NH}_3$  in a 60 cm cell [22, 29] and (ii) on the position of  $\text{H}_2\text{O}$  lines from the HITRAN 2008 database [32]. To compensate for small non-linearities in the laser scanning over a single  $\sim 2\text{ cm}^{-1}$  spectral interval, the relative wavenumber spacing was also simultaneously determined with a free-space Fabry-Perot etalon with a free-spectral range of about  $0.03\text{ cm}^{-1}$ . We estimate the uncertainty in the wavenumber scale to be approximately  $0.001\text{ cm}^{-1}$ . A fraction of the laser light was also used to normalize the laser power over the tuning range (see also Figure 1 in Refs. [22, 29]). In Ref. [22] the mirror reflectivity was determined prior to measurements with formaldehyde based on the known integrated line strengths [32] of selected absorption lines of  $\text{CO}_2$  and  $\text{H}_2\text{O}$  in the relevant spectral region. The un-

certainty of  $(1 - R)$ , which was estimated to be  $\pm 5\%$ , is important for the absolute accuracy of the evaluation of absolute cross-sections as discussed in Section 4. For the new absorption data in the 6804–7051 cm<sup>-1</sup> region the weak wavelength dependence of the mirror reflectivity (as measured by the manufacturer) was used to correct for the weak spectral dependence of  $R$  over the entire wavenumber region. The new absorption spectrum was then matched to the spectrum by Staak et al. in the overlap region (approximately 4 cm<sup>-1</sup> wide) based on a least square procedure and subsequently scaled to the appropriate values. The entire spectrum was corrected by a factor of 2 as recommended in Section 4.

CH<sub>2</sub>O was prepared by pyrolysis of paraformaldehyde (Aldrich, 95% pure) under vacuum. Since water vapour acts as catalyst for the polymerization of CH<sub>2</sub>O, the gaseous CH<sub>2</sub>O was first passed through a cooling trap below 200 K to remove water vapour and potential polymerization products of CH<sub>2</sub>O. The monomeric CH<sub>2</sub>O was then trapped and stored at 77 K under vacuum. The sample cavity was evacuated to approximately 10<sup>-6</sup> mbar (Turbovac 50, Leybold), ensuring that it was virtually free of gaseous water. CH<sub>2</sub>O gas was introduced into the cavity by slowly heating the solid CH<sub>2</sub>O in the cooling trap until a pressure of 2 mbar was reached. The pressure in the cavity was measured with an absolute capacitance manometer (Ceravac CTR100, Leybold; operating range 10<sup>-2</sup> to 120 mbar) with a relative precision of 0.01 mbar. All measurements were taken at a pressure of 2 mbar of CH<sub>2</sub>O. The temperature of the system was 291 ± 2 K.

### 3 Results

The absorption spectrum of CH<sub>2</sub>O from 6547 to 7051 cm<sup>-1</sup> is shown in Figure 1<sup>1</sup>. The spectral data shown in blue has been taken from Staak et al. [22], the green trace represents (as of yet) unpublished data. The maximum signal-to-noise ratio of the spectrum is greater than 500, and more than 4500 lines larger than  $5 \times 10^{-23}$  cm<sup>2</sup> were observed in the spectral region shown. Even though the absorption structure has been largely spectrally resolved, the high density of states of overlapping ro-vibrational combination bands in that region produces a congested spectrum, which makes individual line assignment a formidable task. At room temperature the rotational envelopes of the fundamental modes are slightly wider than ~100 cm<sup>-1</sup> [33], which roughly applies to the combination

---

<sup>1</sup> The spectrum in Figure 1 has two gaps near the low energy end of the region covered (i.e. from 6549.7–6551.3 cm<sup>-1</sup> and 6553.5–6554.5 cm<sup>-1</sup>).

**Table 1:** Combination bands between 6500 and 7050 cm<sup>-1</sup> from the dispersed fluorescence spectra of Bouwens et al. [23].

Combination band	Symmetry <sup>#</sup>	Wavenumber [cm <sup>-1</sup> ]
3 <sub>2</sub> 4 <sub>2</sub> 6 <sub>1</sub>	b <sub>2</sub>	6508.8
1 <sub>1</sub> 3 <sub>1</sub> 4 <sub>2</sub>	a <sub>1</sub>	6562.7
2 <sub>1</sub> 4 <sub>2</sub> 6 <sub>2</sub>	a <sub>1</sub>	6578.8
1 <sub>2</sub> 4 <sub>1</sub>	b <sub>1</sub>	6611.6
3 <sub>1</sub> 4 <sub>2</sub> 5 <sub>1</sub>	b <sub>2</sub>	6635.7*
2 <sub>3</sub> 3 <sub>1</sub>	a <sub>1</sub>	6652.2
2 <sub>1</sub> 3 <sub>1</sub> 4 <sub>3</sub>	b <sub>1</sub>	6693.4*
3 <sub>1</sub> 4 <sub>1</sub> 5 <sub>1</sub> 6 <sub>1</sub>	b <sub>1</sub>	6710.0
3 <sub>1</sub> 5 <sub>1</sub> 6 <sub>2</sub>	b <sub>2</sub>	6759.0
2 <sub>1</sub> 3 <sub>1</sub> 4 <sub>2</sub> 6 <sub>1</sub>	b <sub>2</sub>	6777.6*
4 <sub>1</sub> 5 <sub>2</sub>	b <sub>1</sub>	6795.1
3 <sub>3</sub> 4 <sub>2</sub>	a <sub>1</sub>	6815.2
1 <sub>1</sub> 2 <sub>1</sub> 4 <sub>2</sub>	b <sub>1</sub>	6825.5
2 <sub>1</sub> 3 <sub>1</sub> 4 <sub>1</sub> 6 <sub>2</sub>	b <sub>1</sub>	6849.7
2 <sub>1</sub> 4 <sub>2</sub> 5 <sub>1</sub>	b <sub>2</sub>	6856.3*
2 <sub>4</sub>	a <sub>1</sub>	6864.3*
5 <sub>2</sub> 6 <sub>1</sub>	b <sub>2</sub>	6864.6
2 <sub>1</sub> 3 <sub>1</sub> 6 <sub>3</sub>	b <sub>2</sub>	6894.6
4 <sub>6</sub>	a <sub>1</sub>	6909.0
2 <sub>2</sub> 4 <sub>3</sub>	b <sub>1</sub>	6910.7
1 <sub>1</sub> 2 <sub>1</sub> 4 <sub>1</sub> 6 <sub>1</sub>	(a <sub>2</sub> )	6921.3
2 <sub>1</sub> 4 <sub>1</sub> 5 <sub>1</sub> 6 <sub>1</sub>	b <sub>1</sub>	6964.1
2 <sub>2</sub> 4 <sub>2</sub> 6 <sub>1</sub>	b <sub>2</sub>	7030.7
4 <sub>5</sub> 6 <sub>1</sub>	(a <sub>2</sub> )	7036.0
2 <sub>1</sub> 3 <sub>2</sub> 4 <sub>2</sub>	a <sub>1</sub>	7037.5
2 <sub>1</sub> 5 <sub>1</sub> 6 <sub>2</sub>	b <sub>2</sub>	7048.0

<sup>#</sup> Point group C<sub>2v</sub>: z-axis = C<sub>2</sub>, y-axis in-plane, x-axis normal to plane. a<sub>2</sub> forbidden in C<sub>2v</sub>.

\* Tentative identification of combination bands observed in the spectrum.

bands shown here. The maximum absorption is gradually decreasing over this wavenumber region due to an increasing Franck-Condon inhibition of transitions with increasing energy.

A ro-vibrational structure of combination bands and overtones is apparent across the entire spectrum. However, a comprehensive spectral analysis will be necessary to deconvolute the overlapping combination bands and to assign vibrational bands with confidence. Such an analysis is beyond the scope of this publication. A list of vibrational states occurring in the spectral range is given in

**Table 2:** Wavenumber peak positions [cm<sup>-1</sup>] and corresponding cross-sections per molecule [10<sup>-22</sup> cm<sup>2</sup>/molecule] in the region 6547 cm<sup>-1</sup> to 7051 cm<sup>-1</sup> greater than 3 × 10<sup>-22</sup> cm<sup>2</sup>/molecule. Wavenumber uncertainty is in the last digit. σ<sub>peak</sub>'s are corrected by a factor of 2 (see recommendation in Section 4). # Potential overlap with a H<sub>2</sub>O line.

̄ <sub>peak</sub> [cm <sup>-1</sup> ]	10 <sup>22</sup> σ <sub>peak</sub> [cm <sup>2</sup> molecule]	̄ <sub>peak</sub> [cm <sup>-1</sup> ]	10 <sup>22</sup> σ <sub>peak</sub> [cm <sup>2</sup> molecule]	̄ <sub>peak</sub> [cm <sup>-1</sup> ]	10 <sup>22</sup> σ <sub>peak</sub> [cm <sup>2</sup> molecule]	̄ <sub>peak</sub> [cm <sup>-1</sup> ]	10 <sup>22</sup> σ <sub>peak</sub> [cm <sup>2</sup> molecule]
6567.401	3.66	6641.673	3.73	6698.758	4.39	6781.956	4.56
6567.418	3.07	6642.355	3.44	6701.165	4.93	6783.441	3.41
6576.402	3.03	6644.016	3.16	6703.557	3.64	6784.212	4.38
6576.425	3.92	6644.853	4.33	6730.102	3.23	6786.020	3.80
6595.268	3.25	6646.361	4.40	6732.041	3.91	6786.457	3.98
6598.323	4.34	6647.331	3.94	6732.369	3.32	6788.603	4.76
6598.359	5.05	6648.712	5.34	6734.362	4.19	6788.699	4.27
6600.261	4.94	6649.769	4.46	6734.689	4.23	6790.930	3.11
6601.348	4.45	6651.068	4.46	6736.676	4.40	6791.191	4.37
6602.345	5.00	6652.157	4.52	6737.044	3.92	6793.169	4.21
6604.210	5.91	6652.260	3.02	6738.998	4.84	6793.779	4.23
6604.510	5.04	6652.368	3.32	6739.425	4.11	6795.409	4.48
6606.723	5.65	6653.443	5.04	6741.336	4.24	6795.958	3.32
6606.964	5.60	6654.458	3.60	6741.819	3.91	6796.369	4.14
6607.741	3.06	6655.834	5.23	6743.691	4.88	6797.668	3.70
6608.974	5.51	6656.654	3.91	6744.231	4.75	6798.952	3.79
6609.622	6.76	6658.251	3.93	6746.066	3.82	6799.956	3.63
6611.257	6.91	6658.718	3.22	6746.640	5.34	<u>6802.281</u>	<u>3.96</u>
6612.211	7.01	6659.808	3.25	6748.460	4.47	6828.639	3.01
6613.559	4.18	6659.828	3.24	6749.056	4.19	6885.374	3.97
6614.757	5.89	6660.711	4.15	6750.867	5.09	6885.399	3.42
6615.878	5.21	6662.283	3.90	6751.471	4.34	6885.429	3.81
6617.276	5.64	6663.242	3.43	6753.294	4.53	6885.470	3.37
6618.210	5.23	6664.739	5.08	6753.884	4.18	6885.579	3.40
6619.781	4.54	6667.186	4.38	6755.735	3.70	6885.594	3.11
6620.550	4.39	6669.625	3.07	6756.286	3.58	6971.278#	4.43
6622.281	3.77	6681.774	7.47	6758.682	4.44	6971.327	3.47
6622.896	3.73	6693.920	3.35	6777.411	3.10	6971.354	3.19
6624.779	4.55	6695.399	4.07	6779.693	3.73	6993.244	3.21
6639.845	3.02	6696.342	3.23	6780.872	3.59		

Table 1, which is based on a list of combination and overtone bands reported by Bouwens et al. [23]. States whose occurrence in the spectrum is apparent on basis of apparent branch structures are marked with an asterisk in Table 1.

The strongest absorption lines in the spectrum (those with absorption cross-sections greater than 3 × 10<sup>-22</sup> cm<sup>2</sup>) are listed in Table 2. This cut-off criterion results in 120 lines. The spectrum is not entirely free of H<sub>2</sub>O lines, especially the

new data from 6804–7051 cm<sup>-1</sup> (indicated by the bold line in Table 2) . In this region the spectral density of water absorption features is increasing and due to the fact that the laser beam travelled outside the cavity in ambient air for more than 2 m the strongest H<sub>2</sub>O lines ( $> 1 \times 10^{-23}$  cm/molecule) are observable in the spectrum. The entire spectrum is available in the supplementary material.

## 4 Discussion and critical review of cross-sections from 6547–7051 cm<sup>-1</sup>

Since Staak et al. [22] published the absorption spectrum of CH<sub>2</sub>O in the range 6547–6804 cm<sup>-1</sup>, several research groups have used individual lines in this wavelength range for quantification of CH<sub>2</sub>O in different chemical systems using cw-cavity ring-down spectroscopy (cw-CRDS). In all experiments it turned out, that the results could not be explained in a satisfactory way if the absorption cross-sections as published by Staak et al. [22] were employed. Some direct measurements of the absorption cross-sections of a few absorption lines have been undertaken since the work of Staak et al., and have found smaller absolute values for the absorption cross-sections.

In the following, the different chemical systems together with their conclusions concerning the CH<sub>2</sub>O absorption cross-sections will be briefly reviewed, for more details on the experimental techniques or the data analysis, the reader is referred to the original literature. The absorption cross-sections deduced from all experiments are summarized in Table 3.

### 4.1 Photolysis of CH<sub>3</sub>ONO in a large photo-reactor [24]

The photolysis of CH<sub>3</sub>ONO in the UV is a common source for OH radicals in atmospheric simulation chambers: the initially formed CH<sub>3</sub>O radical leads, in the presence of O<sub>2</sub>, to the rapid formation of HO<sub>2</sub> and CH<sub>2</sub>O, whereby HO<sub>2</sub> reacts subsequently with the co-product NO to form OH radicals. HONO is a possible by-product in this system from the reaction of OH with NO. Djehiche et al. [24] studied the photolysis of CH<sub>3</sub>ONO at a total pressure of 53.3 mbar of air in a 140 dm<sup>3</sup> photo-reactor equipped with a cw-CRDS detection system. The primary goal of this study was the direct observation of HONO formation, suspected to be a direct product of the reaction of OH radicals with CH<sub>3</sub>ONO. The build-up of CH<sub>2</sub>O and HONO were measured simultaneously in a time resolved way by cw-CRDS following the continuous UV irradiation of a known concentration

**Table 3:** Line positions ( $\tilde{\nu}$ ), line strengths ( $S$ ) and absorption cross-sections ( $\sigma$ ) as they were evaluated in different experiments in the literature. The 3<sup>rd</sup> column shows the line strength  $S_{\text{Staak}}$  from Ref. [22] as reported in the publications stated in the 6<sup>th</sup> column. As Staak et al. published absorption coefficients  $\sigma$  at 2 mbar CH<sub>2</sub>O, these values were converted by the authors of Refs. [24, 26, 28] into line strength  $S$  using a Voigt profile and the broadening coefficients given in Ref. [22]. The 4<sup>th</sup> and 5<sup>th</sup> column summarize the values as published in the corresponding reference in the 6<sup>th</sup> column, i.e. the absorption cross sections for experimental conditions used in the corresponding studies, and sometimes the line strength calculated using a Voigt profile and appropriate broadening coefficients.

Experiment	$\tilde{\nu}$ [cm <sup>-1</sup> ]	$10^{23} S_{\text{Staak}}$ Ref. [22] [cm <sup>-1</sup> molecule <sup>-1</sup> ]	$10^{23} S$ [cm <sup>-1</sup> molecule <sup>-1</sup> ]	$10^{22} \sigma$ [cm <sup>2</sup> molecule <sup>-1</sup> ]	Ref.
From photolysis of CH <sub>3</sub> ONO at 53.3 mbar air (Section 4.1)	6625.74	0.21	0.12	0.27	[24]
From low temperature oxidation of CH <sub>4</sub> (Section 4.2)	6638.78			5.1	[25]
	6638.80			5.2	
	6641.67			7.8	
	6642.36			7.2	
From OH reaction kinetics (Section 4.3)	6624.78	1.84	0.91	5.3/4.2	[26]
	6625.25	1.05	0.52	3.2/2.5	
From n-butane oxidation in jet-stirred reactor (Section 4.4)	6624.78			5.34	[27]
	6625.25			3.20	
	6639.33			3.60	
	6641.67			4.59	
	6642.35			4.24	
	6642.49			1.52	
From equilibrium reaction of HO <sub>2</sub> + CH <sub>2</sub> O (Section 4.5)	6625.25	1.05	0.52	2.47	[28]

of CH<sub>3</sub>ONO with various numbers of fluorescing tubes. CH<sub>2</sub>O is, in 53.3 mbar of air, a primary product of the photolysis of CH<sub>3</sub>ONO, and therefore the rise of the CH<sub>2</sub>O concentration can be used to deduce the photolysis frequency. CH<sub>2</sub>O was detected at a wavenumber of 6625.74 cm<sup>-1</sup>, close to an intense absorption line of HONO. In a first attempt, the CH<sub>2</sub>O concentration was determined using absorption cross-section  $\sigma_{2 \text{ mbar}}$  as published by Staak et al. Djehiche et al. used CH<sub>2</sub>O in 53.3 mbar air, therefore  $\sigma_{2 \text{ mbar}}$  had to be converted into  $\sigma_{53 \text{ mbar}}$ . For this purpose, the value  $\sigma_{2 \text{ mbar}} = 1.07 \times 10^{-22} \text{ cm}^2 \text{ molecule}^{-1}$  was first converted into the corresponding line strength ( $S = 2.1 \times 10^{-24} \text{ cm}^{-1}/\text{molecule cm}^{-2}$ ) using

Voigt profiles and the self-broadening coefficients  $\gamma_{\text{self}}$  from Staak et al. ( $\gamma_{\text{self}} = 9.18 \times 10^{-4} \text{ cm}^{-1} \text{ mbar}^{-1}$ ). Subsequently the  $\text{CH}_2\text{O}$  absorption cross-section  $\sigma_{53 \text{ mbar}} = 5.5 \times 10^{-23} \text{ cm}^2 \text{ molecule}^{-1}$  was calculated using again a Voigt profile and the  $\text{N}_2$ -broadening coefficient ( $\gamma_{\text{N}_2} = 2.35 \times 10^{-4} \text{ cm}^{-1} \text{ mbar}^{-1}$ ). Based on this absorption cross-section  $\sigma_{53 \text{ mbar}}$ , the obtained  $\text{CH}_3\text{ONO}$  photolysis frequencies were not in line with the values expected from other systems. Therefore the  $\text{CH}_2\text{O}$  absorption cross-section was re-measured directly again at  $6625.74 \text{ cm}^{-1}$  using a mixture from a standard cylinder of  $\text{CH}_2\text{O}$  in zero-air whose calibration mixing ratio was validated with the DNPH-HPLC method [16] to be 40 ppmv. The reactor was filled with 53.3 mbar of this gas mixture and the peak absorption cross-section of  $2.7 \times 10^{-23} \text{ cm}^2 \text{ molecule}^{-1}$  at  $6625.74 \text{ cm}^{-1}$  was measured. For comparison this value can be transformed into a line strength by using  $\text{N}_2$  broadening coefficient from Staak et al.. The obtained value ( $\sigma = 1.2 \times 10^{-24} \text{ cm}^2 \text{ molecule}^{-1}$ ) turned out to be a factor of  $\sim 2$  smaller than that by Staak et al.

## 4.2 Low temperature combustion of $\text{CH}_4$ [25]

The methane oxidation has been investigated under low temperature combustion conditions using a jet-stirred reactor (JSR) coupled to a cw-CRDS cavity [25, 27, 34]. The gas mixture was continuously pumped through a small orifice from the JSR, kept at atmospheric pressure, into a CRDS cavity, which was kept at a pressure of ca. 13.3 mbar. The absorption spectrum was measured using CRDS in the wavelength range 6638 to  $6642.5 \text{ cm}^{-1}$ , allowing the selective quantification of several species ( $\text{CH}_4$ ,  $\text{H}_2\text{O}$  and  $\text{CH}_2\text{O}$ )<sup>2</sup>, while many other species have been detected simultaneously by gas chromatography (GC). Good agreement for the  $\text{CH}_4$  concentrations obtained by both methods give confidence in the determination of the CRDS absorption path length. In a typical *single* experiment the JSR is kept at a constant temperature and the absorption spectrum of the reaction products is measured over a given wavelength range. A measurement of that kind takes typically 10 to 20 min, over which the gas mixture is continuously pumped through the ring-down cavity with a flow rate of around  $90 \text{ cm}^3 \text{ min}^{-1}$ , leading to a residence time of the gas mixture within the CRDS cell of around 0.3 s. Due to these flow conditions, possible absorption of  $\text{CH}_2\text{O}$  on the walls of the CRDS cavity is probably in equilibrium with the gas phase and was therefore considered negligible. A complete experiment consisted of several *single* experiments at different temperatures with the goal of observing the resulting change in concen-

---

<sup>2</sup> Note that  $\text{H}_2\text{O}$  and  $\text{CH}_2\text{O}$  are difficult to be quantified by gas chromatography.

tration of the oxidation products with temperature. Experiments can then be performed using different initial reactant concentrations or residence times within the JSR. Chemical models, incorporating hundreds of species and chemical reactions, can then be developed to reproduce the species' time profiles as good as possible.

In the experiment in Ref. [25], CH<sub>2</sub>O was quantified using 4 different absorption lines at 6638.777 cm<sup>-1</sup>, 6638.804 cm<sup>-1</sup>, 6641.674 cm<sup>-1</sup> and 6642.355 cm<sup>-1</sup> whereby absorption cross-sections of 5.1, 5.2, 7.8, and  $7.2 \times 10^{-22}$  cm<sup>2</sup> molecule<sup>-1</sup>, respectively, were directly taken from Staak et al. [22]. This simplification was based on the assumption that the pressure broadening at 13.3 mbar of the gas mixture in the CRDS cell (consisting of 0.84 mbar CH<sub>4</sub>, 0.84 mbar O<sub>2</sub> and 11.6 mbar He) is similar to the pressure broadening of the 2 mbar of pure CH<sub>2</sub>O as used by Staak et al. Subsequent modelling of the combustion chemistry overestimated the CH<sub>2</sub>O concentration by ca. a factor of ~1.7, i.e. the measured concentrations were lower than predicted by the model. This was surprising because the oxidation chemistry of CH<sub>4</sub> is well known and the model was expected to reproduce the CH<sub>2</sub>O concentration. Decreasing the absorption cross-section used to transform ring-down times into concentrations by a factor of 2 compared to the values obtained by Staak et al. would bring model and measurement into good agreement.

### 4.3 Indirect measurement of the absorption cross-sections [26]

Morajkar et al. [26] measured absorption cross-sections of two absorption lines of CH<sub>2</sub>O using a laser photolysis reactor equipped with a cw-CRDS apparatus and a high repetition rate laser induced fluorescence (LIF) setup [35]. The absorption cross-sections of the lines at 6624.779 and 6625.248 cm<sup>-1</sup> were quantified at ≈ 13.3 and ≈ 66.1 mbar helium. A major difficulty in handling CH<sub>2</sub>O is that it is easily adsorbed on surfaces and that it also tends to polymerize (see Section 4.6). Therefore, the time-resolved pseudo-first order decay of OH radicals was measured by LIF in combination with simultaneous cw-CRDS measurements of two CH<sub>2</sub>O absorption lines. In excess of CH<sub>2</sub>O, OH radical concentrations will decrease exponentially due to the reaction OH + CH<sub>2</sub>O → H<sub>2</sub>O + HCO. Based on the rate coefficient of this reaction, which is known to within 15% [36], the CH<sub>2</sub>O concentration within the photolysis reactor can be evaluated. Through the simultaneous absorption measurement the line strengths for the lines at 6624.779 and 6625.248 cm<sup>-1</sup> were thus determined to be  $S = 9.1$  and  $5.2 \times 10^{-24}$  cm<sup>-1</sup>/molecule cm<sup>-2</sup>, respectively, assuming Voigt profiles.

These line strengths are again a factor of  $\approx 2$  smaller than those in Staak et al. (i.e.  $S = 18.4$  and  $10.5 \times 10^{-23} \text{ cm}^{-1}/\text{molecule cm}^{-2}$  respectively), which were deduced from the peak absorption cross-sections and the self-broadening coefficient from Ref. [22].

#### 4.4 Low temperature oxidation of n-butane in a JSR [27]

Similar to the experiment concerning  $\text{CH}_4$  oxidation [25] (Section 4.2) the low temperature oxidation of n-butane [27] (and very recently on the oxidation of Dimethylether [37]) was investigated in a JSR. During this experiment  $\text{CH}_2\text{O}$  concentrations were determined using six different lines: 6624.78, 6625.25, 6639.33, 6641.67, 6642.35, and 6642.49  $\text{cm}^{-1}$ . Two of these lines (*in italic*) had been measured by Morajkar et al. [26] and two others (underlined) were previously used in the  $\text{CH}_4$  experiments [25]. During some of the experiments,  $\text{CH}_2\text{O}$  had also been quantified by GC using a methanizer (by catalytically converting  $\text{CH}_2\text{O}$  into  $\text{CH}_4$ , which can be detected with greater sensitivity). The  $\text{CH}_2\text{O}$  concentration profiles obtained from the two lines measured by Morajkar et al. [26] were in good agreement with the GC measurements in Ref. [27] as well as with model predictions, while the profiles from the other four lines, taking absorption cross-sections from Ref. [22] (such as has been done in Ref. [25]) lead to concentrations that were on average lower by a factor of 1.7; i.e. best agreement was obtained by dividing the peak absorption cross-sections from [22] by a factor of 1.7. Considering a Voigt profile and the differences in pressure broadening (13.2 mbar Helium for JSR conditions compared to 2 mbar  $\text{CH}_2\text{O}$  for Staak et al. conditions, with broadening coefficient of 0.04 and  $0.93 \text{ cm}^{-1}/\text{atm}$  for He and  $\text{CH}_2\text{O}$ , respectively), leads to a factor of 2 lower line strength.

#### 4.5 Equilibrium constant of the reaction of $\text{CH}_2\text{O}$ with $\text{HO}_2$ [28]

In a study to determine the equilibrium constant of the reaction of  $\text{CH}_2\text{O}$  with  $\text{HO}_2$  radicals [28] the formaldehyde cross-sections were also evaluated. For these kinetic experiments, low concentrations of  $\text{HO}_2$  were generated by photolysing  $\text{CH}_2\text{O}$  in the presence of  $\text{O}_2$  and  $\text{HO}_2$  concentrations were monitored by time-resolved cw-CRDS. The absolute  $\text{CH}_2\text{O}$  concentrations were determined before each experiment by means of the absorption line at 6625.248  $\text{cm}^{-1}$ , the same line that was used in Refs. [26, 27]. As only a very small fraction of  $\text{CH}_2\text{O}$  is being photolysed,  $\text{HO}_2$  radicals decay exponentially under pseudo-first order conditions through their reaction with  $\text{CH}_2\text{O}$ . At appropriate temperatures, the adduct

is unstable and the reverse reaction, the decomposition of HO<sub>2</sub>CH<sub>2</sub>O, becomes important. Under these conditions it was observed that the time-dependent concentrations of HO<sub>2</sub> did not decay to zero; instead an equilibrium concentration was reached at long reaction times. The fraction of this residual HO<sub>2</sub> concentration compared to the initial concentration is given by the equilibrium constant and depends, at a given temperature, only on the absolute CH<sub>2</sub>O concentration. In other words, the equilibrium constant deduced from the time-resolved, relative HO<sub>2</sub> concentrations are directly dependent on the absorption cross-sections used for converting ring-down times into CH<sub>2</sub>O concentrations. By using the absorption cross-sections as obtained by Morajkar et al. [26] for CH<sub>2</sub>O quantification (i.e.  $2.47 \times 10^{-22}$  cm<sup>-2</sup> molecule<sup>-1</sup>) at 6625.248 cm<sup>-1</sup> at 66.6 mbar Helium), excellent agreement of the equilibrium constant was found in comparison to earlier literature values [38, 39], which were obtained by different techniques. This is indirect confirmation that the smaller absorption cross-sections appear to be correct.

## 4.6 Possible explanation for disagreement

No simple explanation for the systematically higher values obtained by Staak et al. compared to other studies [24–28] can be given, as different reasons might be involved.

In order to compare the values reported by different publications, absorption cross-sections measured by Staak et al. in 2 mbar CH<sub>2</sub>O had to be converted into absorption cross-sections that apply to the experimental conditions used in the different experiments in the literature (typically highly diluted CH<sub>2</sub>O in a few mbar Helium and up to 50 mbar air). For this purpose, appropriate Voigt profiles were assumed and broadening coefficients as determined for selected lines by Staak et al. Since broadening coefficients depend on the quantum numbers pertinent to the relevant transitions [40] it is conceivable that the applied broadening coefficients contain a small systematic error. However, as a consistent deviation of a factor of 2 was found regardless the experimental conditions, systematic errors in the broadening coefficients are unlikely to cause the discrepancy.

Staak et al. have measured the spectrum in a static cell, filling it with 2 mbar of CH<sub>2</sub>O. Even though a systematic error in the pressure measurement with an absolute capacitance gauge might not be ruled out completely, it appears unlikely to be the sole cause for the observed cross-section differences. On its own the potential error in pressure is too small to account for the size (factor 2) of the discrepancy. Polymerization of CH<sub>2</sub>O at 2 mbar as a reason for biasing the pressure measurement appears to be negligible.

Since  $\text{CH}_2\text{O}$  is “sticky” and generally difficult to handle,  $\text{CH}_2\text{O}$  can potentially adsorb on the cavity mirrors of the sample cell, thus adding to the light absorption, but not to the pressure measurement. Such an effect would lead to higher absorption cross-sections owing to a reduced mirror reflectivity. The methods used in Refs. [24–28] are based on kinetics measurements in conjunction with flow cell setups where equilibrium conditions are less critical to establish and wall losses of formaldehyde are minimized. Another reason might be that in CEAS, the reflectivity of the mirrors must be obtained through independent experiments in order to determine absolute cross-sections. In that sense CEAS is not an “absolute” method as opposed to CRDS where, firstly, knowledge of the exact cavity mirror reflectivity is not required to determine absolute cross-sections, and secondly mirror reflectivities can be directly determined from simple reference measurements without sample. Hence reflectivity calibration measurements as they are usually performed in CEAS (e.g. with a gas of known absorption cross-section and number density) are not necessary. All systematic errors during the calibration of the mirror reflectivity in CEAS can have an impact on the absorption cross-sections of  $\text{CH}_2\text{O}$ . Therefore, we think that it cannot be ruled out that the sum of all possible errors in the work of Staak et al. might lead to cross-sections that are systematically too high by a factor of 2.

## 5 Conclusion and recommendation

The formaldehyde absorption spectrum from Staak et al. has been extended to cover the region 6547 to  $7051\text{ cm}^{-1}$ ; the published absolute cross-sections in that region have been reviewed. The new region covered here ( $6804$ – $7051\text{ cm}^{-1}$ ) is not entirely free of water absorption features. The cross-sections in Figure 1, in Table 2, and in the supplementary material have all been corrected to smaller values in accordance with the review of literature data in Section 4. We recommend using the new data from this publication in future work rather than the original data in Ref. [22], as far as cross-sections are concerned. Please note that there have been no indications that relative lines strengths in Ref. [22] are overly biased, and neither discrepancies in the stated accuracy of line positions nor in the reported broadening coefficients are evident.

**Acknowledgement:** This project was supported by the French ANR agency under contract No. ANR-11-LabEx-0005-01 CaPPA (Chemical and Physical Properties of the Atmosphere). Support through SFI’s Research Frontier Programme (Contract: 11/RFP.1/PHY/3233) is gratefully acknowledged.

## References

1. G. K. Moortgat, W. Seiler, and P. Warneck, *J. Photoch.* **17** (1981) 139.
2. R. Atkinson, D. L. Baulch, R. A. Cox, R. F. Hampson Jr., J. A. Kerr, M. J. Rossi, and J. Troe, *J. Phys. Chem. Ref. Data* **26** (1997) 521.
3. M. C. Cooke, S. R. Utembe, P. Gorrotxategi Carbajo, A. T. Archibald, A. J. Orr-Ewing, M. E. Jenkin, R. G. Derwent, D. J. Lary, and D. E. Shallcross, *Atmos. Sci. Lett.* **11** (2010) 33.
4. C. Y. Lee, Y. J. Kim, S. B. Hong, H. Lee, J. S. Jung, Y. J. Choi, J. Park, K. H. Kim, J. H. Lee, K. J. Chun, and H. H. Kim, *Water Air Soil Poll.* **166** (2005) 181.
5. U. Platt and D. Perner, *J. Geophys. Res.-Atmos.* **85** (1980) 7453.
6. K. Chance, P. I. Palmer, R. J. D. Spurr, R. V. Martin, T. P. Kurosu, and D. J. Jacob, *Geophys. Res. Lett.* **27** (2000) 3461.
7. A. Heckel, A. Richter, T. Tarsu, F. Wittrock, C. Hak, I. Pundt, W. Junkermann, and J. P. Burrows, *Atmos. Chem. Phys.* **5** (2005) 909.
8. M. Grutter, E. Flores, G. Andraca-Ayala, and A. Baez, *Atmos. Environ.* **39** (2005) 1027.
9. R. J. Yokelson, J. G. Goode, D. E. Ward, R. A. Susott, R. E. Babbitt, D. D. Wade, I. Bertschi, D. W. T. Griffith, and W. M. Hao, *J. Geophys. Res.-Atmos.* **104** (1999) 30109.
10. V. Wagner, C. Schiller, and H. Fischer, *J. Geophys. Res.-Atmos.* **106** (2001) 28529.
11. A. Fried, B. P. Wert, B. Henry, and J. R. Drummond, *Spectrochim. Acta A* **55** (1999) 2097.
12. H. Dahnke, G. von Basum, K. Kleinermanns, P. Hering, and M. Mürtz, *Appl. Phys. B-Lasers O.* **75** (2002) 311.
13. A. Gratien, B. Picquet-Varrault, J. Orphal, E. Perraudin, J.-F. Doussin, and J.-M. Flaud, *J. Geophys. Res.* **112** (2007) D05305.
14. V. Catoire, F. Bernard, Y. Mebarki, A. Mellouki, G. Eyglunent, V. Daele, and C. Robert, *J. Environ. Sci.-China* **24** (2012) 22.
15. J. Cihelka, I. Matulkova, and S. Civis, *J. Mol. Spectrosc.* **256** (2009) 68.
16. B. Hanoune, T. LeBris, L. Allou, C. Marchand, and S. Le Calve, *Atmos. Environ.* **40** (2006) 5768.
17. P. Devolder, S. Dusanter, B. Lemoine, and C. Fittschen, *Chem. Phys. Lett.* **417** (2006) 154.
18. H. R. Barry, L. Corner, G. Hancock, R. Peverall, T. L. Ranson, and G. A. D. Ritchie, *Phys. Chem. Chem. Phys.* **5** (2003) 3106.
19. H. Barry, L. Corner, G. Hancock, R. Peverall, and G. A. D. Ritchie, *Phys. Chem. Chem. Phys.* **4** (2002) 445.
20. L. Corner, H. R. Barry, and G. Hancock, *Chem. Phys. Lett.* **374** (2003) 28.
21. W. Zhao, X. Gao, L. Deng, T. Huang, T. Wu, and W. Zhang, *J. Quant. Spectrosc. Ra.* **107** (2007) 331.
22. M. Staak, E. W. Gash, D. S. Venables, and A. A. Ruth, *J. Mol. Spectrosc.* **229** (2005) 115.
23. R. J. Bouwens, J. A. Hammerschmidt, M. M. Grzeskowiak, T. A. Stegink, P. M. Yorba, and W. F. Polik, *J. Chem. Phys.* **104** (1996) 460.
24. M. Djehiche, A. Tomas, C. Fittschen, and P. Coddeville, *Environ. Sci. Technol.* **45** (2011) 608.
25. C. Bahrini, O. Herbinet, P.-A. Glaude, C. Schoemaecker, C. Fittschen, and F. Battin-Leclerc, *Chem. Phys. Lett.* **534** (2012) 1.
26. P. Morajkar, C. Schoemaecker, and C. Fittschen, *J. Mol. Spectrosc.* **281** (2012) 18.
27. C. Bahrini, P. Morajkar, C. Schoemaecker, O. Frottier, O. Herbinet, P.-A. Glaude, F. Battin-Leclerc, and C. Fittschen, *Phys. Chem. Chem. Phys.* **15** (2013) 19686.

28. P. Morajkar, C. Schoemaecker, M. Okumura, and C. Fittschen, Int. J. Chem. Kinet. **46** (2014) 245.
29. D. M. O'Leary, J. Orphal, A. A. Ruth, U. Heitmann, P. Chelin, and C. E. Fellows, J. Quant. Spectrosc. Ra. **109** (2008) 1004.
30. D. M. O'Leary, A. A. Ruth, S. Dixneuf, J. Orphal, and R. Varma, J. Quant. Spectrosc. Ra. **113** (2012) 1138.
31. J. B. Paul, L. Lapson, and J. G. Anderson, Appl. Opt. **40** (2001) 4904.
32. L. S. Rothman, I. E. Gordon, A. Barbe, D. C. Benner, P. F. Bernath, M. Birk, V. Boudon, L. R. Brown, A. Campargue, J.-P. Champion, K. Chance, L. H. Coudert, V. Dana, V. M. Devi, S. Fally, J.-M. Flaud, R. R. Gamache, A. Goldman, D. Jacquemart, I. Kleiner, N. Lacome, W. J. Lafferty, J.-Y. Mandin, S. T. Massie, S. N. Mikhailenko, C. E. Miller, N. Moazzen-Ahmadi, O. V. Naumenko, A. V. Nikitin, J. Orphal, V. I. Perevalov, A. Perrin, A. Predoi-Cross, C. P. Rinsland, M. Rotger, M. Šimecková, M. A. H. Smith, K. Sung, S. A. Tashkun, J. Tennyson, R. A. Toth, A. C. Vandaele, and J. Vander Auwera, J. Quant. Spectrosc. Ra. **110** (2009) 533.
33. G. Herzberg, *Molecular spectra and molecular structure: Vol. II. Infrared and Raman spectra of polyatomic molecules*, D. Van Nostrand Company, Inc., Princeton 1968.
34. C. Bahrini, O. Herbinet, P.-A. Glaude, C. Schoemaecker, C. Fittschen, and F. Battin-Leclerc, J. Am. Chem. Soc. **134** (2012) 11944.
35. A. Parker, C. Jain, C. Schoemaecker, P. Sriftgiser, O. Votava, and C. Fittschen, Appl. Phys. B-Lasers O. **103** (2011) 725.
36. R. Atkinson, D. L. Baulch, R. A. Cox, J. N. Crowley, R. F. Hampson, R. G. Hynes, M. E. Jenkin, M. J. Rossi, and J. Troe, Atmos. Chem. Phys. **4** (2004) 1461.
37. A. Rodriguez, O. Frottier, O. Herbinet, R. Fournet, R. Bounaceur, C. Fittschen, and F. Battin-Leclerc, J. Phys. Chem. A **119** (2015) 1905.
38. J. P. Burrows, G. K. Moortgat, G. S. Tyndall, R. A. Cox, M. E. Jenkin, G. D. Hayman, and B. Veyret, J. Phys. Chem. **93** (1989) 2375.
39. B. Veyret, R. Lesclaux, M. T. Rayez, J. C. Rayez, R. A. Cox, and G. K. Moortgat, J. Phys. Chem. **93** (1989) 2368.
40. N. Ibrahim, J. Thiebaud, J. Orphal, and C. Fittschen, J. Mol. Spectrosc. **242** (2007) 64.

---

**Supplementary material:** The online version of this article (DOI: 10.1515/zpch-2015-0623) provides supplementary material for authorized users.